Dyes and Pigments 94 (2012) 88–98

Contents lists available at SciVerse ScienceDirect

Dyes and Pigments

journal homepage: www.elsevier.com/locate/dyepig

Alkyloxy substituted organic dyes for high voltage dye-sensitized solar cell: Effect of alkyloxy chain length on open-circuit voltage

Soo-Byung Ko, An-Na Cho, Mi-Jeong Kim, Chang-Ryul Lee, Nam-Gyu Park*

School of Chemical Engineering and Department of Energy Science, Sungkyunkwan University, Suwon 440-746, Republic of Korea

ARTICLE INFO

Article history:
Received 29 July 2011
Received in revised form
14 October 2011
Accepted 19 October 2011
Available online 2 November 2011

Keywords:
Organic dyes
p-Phenylenevinylene
Alkyloxy chain length
Dye-sensitized solar cell
Open-circuit voltage
Recombination suppression

ABSTRACT

Three novel organic dyes (**SB1**, **SB2**, and **SB3**) containing 4-(hexyloxy)-*N*-(4-(hexyloxy)phenyl)-*N*-phenylaniline as electron donor and cyanoacrylic acid as electron acceptor bridged by alkyloxy (methyl = **SB1**, propyl = **SB2** and hexyl = **SB3**) substituted *p*-phenylenevinylene linkers have been synthesized. Density functional theory (DFT) has employed to study electron distribution and intramolecular charge transfer. Increase in alkyl chain length in alkyloxy substituent leads to increase in open-circuit voltage (V_{OC}), which is found to be related to the increased electron lifetime at open-circuit condition. Under AM 1.5 G 1 sun light illumination (100 mW/cm^2), an optimized **SB3**-sensitized cell show a short-circuit photocurrent density (J_{SC}) of 12.83 mA/cm^2, an open-circuit voltage (V_{OC}) of 0.745 V and a fill factor (*FF*) of 0.64, corresponding to an overall conversion efficiency (η) of 6.12%. Little degradation in η observed over 40 days is indicative of long-term stability of the **SB**-series dyes.

1. Introduction

During the foregone two decades, the dye-sensitized solar cell (DSSC) composed of a dye-adsorbed mesoporous TiO_2 film, a redox electrolyte, and a platinum-coated counter electrode has attracted remarkable attention by virtue of its giant potential as a low-cost solar-to-electrical energy conversion device [1,2]. Promoted by continuous material development as well as device engineering, the cells using polypyridyl ligand coordinated ruthenium complex dyes such as **N3** [1,3], **N719** [4], and **N749** [5] have achieved solar-to-electrical energy conversion efficiency as high as 11% under the standard solar illumination. Although these ruthenium derivatives exhibited high efficiency and good stability [6], they seem to be expensive due to ruthenium metal and hard to purify from the synthetic mixture. Meanwhile, metal-free organic dyes have explored for DSSC because of their wide variety of the structure versatility, and facile modifications for the absorption wavelength range, molar extinction coefficient and HOMO–LUMO energy levels [7]. Generally, π-conjugated bridge structure with electron donor–acceptor moieties has been known to be effective for intramolecular charge transfer, which is suitable for high efficient DSSC applications. To date, various organic dyes including coumarin [8], indoline [9], squaraine [10], polyene [11], hemicyanine [12], oligothiophene [13], perylene [14] porphyrin [15], carbazole [16], benzothidizole [17] and truexene [18] have been developed and attained high efficiency up to 9% [9b,19]. Another derivatives containing triarylamine unit [20] or additional methoxy groups [19b,21] also have been widely studied due to their prominent electron donating ability and hole-transport properties. As part of our efforts to investigate the structural modifications of triarylamine based organic dye, *p*-phenylenevinylene units instead of thiophene chain have been introduced by π-conjugated linker [22]. In particular, organic molecules including oligo(*p*-phenylenevinylene) unit were applied for materials in light-emitting diodes [23] and solar cells [24] owing to their stability and high luminescent efficiency. We previously reported the methoxy substituted phenylenevinylene dye (**TA-DM-CA**), which was developed to enhance the electron donating character in π-conjugated donor–acceptor skeleton, showed an efficiency (η) of 6.49% with short-circuit current density (J_{SC}) of 13.83 mA/cm^2, open-circuit voltage (V_{OC}) of 0.677 V and fill factor (*FF*) of 0.692 [19b–22b]. However, increase in the conjugation length (**TA-TM-CA** and **TA-HM-CA**) led to relatively lower efficiency (5.02% and 5.21%) although their absorption bands shift to longer wavelength, which was due to the decreased V_{OC}.

The performances of DSSCs based on the organic dyes, however, have not exceeded those on the polypyridyl ligand coordinated

* Corresponding author. Tel.: +82 31 290 7241.
E-mail address: npark@skku.edu (N.-G. Park).

0143-7208/$ – see front matter © 2011 Elsevier Ltd. All rights reserved.
doi:10.1016/j.dyepig.2011.10.014

ruthenium complexes yet because of their shorter electron lifetime (τ_r) and intermolecular charge transfer due to dye aggregation, associated with relatively low V_{OC} [7,25]. For overcoming these limitations, our further efforts have been made to increase τ_r and reduce intermolecular charge transfer by structural modification of our previous **TA-DM-CA** dye. We herein report three novel organic dyes (**SB1**, **SB2**, and **SB3**) containing 4-(hexyloxy)-*N*-(4-(hexyloxy) phenyl)-*N*-phenylaniline as electron donor and cyanoacrylic acid as electron acceptor bridged by alkyloxy substituted *p*-phenylenevinylene π-conjugated spacers (Fig. 1). Optical and electrochemical characterization are performed and effect of alkyl chain length in the alkyloxy substituent on photovoltaic performance is investigated. Long-term stability for the SB-series dyes is also reported.

2. Experimental

2.1. Materials

All reagents were obtained from Aldrich unless otherwise specified as received without further purification. Flash column chromatography was carried out on silica gel (Merck; silica gel 60, 230–400 mesh). Anatase TiO_2 nanoparticles were synthesized by acetic acid *via* the catalyzed hydrolysis of titanium isopropoxide (97%, Aldrich), followed by autoclaving at 230 °C for 12 h. An aqueous solvent in the autoclaved TiO_2 colloid solution was replaced by ethanol for preparation of non aqueous TiO_2 paste. Ethyl cellulose (Aldrich), lauric acid (Fluka) and terpineol (Aldrich) were added into the ethanol solution of the TiO_2 particles, and then ethanol was removed from the solution using a rotary evaporator to obtain viscous pastes. For homogeneous mixing, the paste was further treated with three-roll mill. The nominal composition of TiO_2/terpineol/ethylcellulose/lauric acid was 1.25/4/0.3/0.1. **N719** ($TBA_2[RuL_2(NCS)_2]$, where L is 4-carboxylic acid-4′carboxylate-2,2′-bipyridine and TBA is tetrabutylammonium) dye was obtained from Esolar. Compound **TA-DM-CA** was prepared according to the literature procedures [19b–22b].

2.2. General characterization methods

The chemical structures of the materials used in this study were identified by nuclear magnetic resonance (NMR) spectra were recorded on a Varian Unity inova 300 MHz spectrometer. ^{1}H NMR spectra were referenced to tetramethylsilane (TMS, 0.00 ppm) using $CDCl_3$ as solvent. ^{13}C NMR spectra were referenced to solvent carbons (77.16 ppm for $CDCl_3$). High resolution mass spectra which were recorded on a JEOL Ltd JMS-700 mstation obtained by FAB and reported in units of mass to charge (*m*/*z*). The absorption and photoluminescence spectra were recorded on an Agilent 8453 UV–visible spectroscopy and a Riken-Keiki fluorescence spectrometer, respectively. The electrochemical cyclic voltammetry (CV) was measured with a three-electrode electrochemical cell on a Autolab (AUT128N, FRA2) electrochemical analyzer. The measurements were carried out in CH_2Cl_2 solution with tetrabutylammonium hexafluorophosphate (0.1 M) at a scan rate 100 mV/s. Au, Pt and Ag/AgCl were employed as working, counter, and reference electrodes. Under the present experimental conditions, the redox potentials are reported with a ferrocenium/ferrocene (Fc^+/Fc) redox couple as an internal reference (0.46 V *vs* SCE) [26].

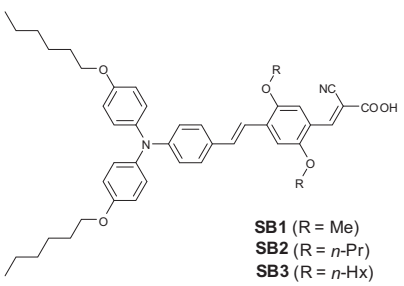

Fig. 1. Molecular structures of the **SB1**, **SB2**, and **SB3** dyes.

2.3. Fabrication and characterization of dye-sensitized solar cells

FTO glasses (Pilkington, TEC-8, 8 Ω/sq) were washed in ethanol using an ultrasonic bath for 10 min. The FTO layer was first covered with 0.1 M Ti(IV) bis(ethyl acetoacetato)diisopropoxide (Aldrich) in 1-butanol (Aldrich) solution by spin-coating method, on which the nanocrystalline TiO_2 paste was deposited using a doctor-blade technique. After the TiO_2 films were heated at 550 °C for 1 h, the sides of TiO_2 films was trimmed to 9 mm wide and 5 mm long. The thickness of TiO_2 films was measured by Alpha step profiler (KLA-Tencor). The annealed TiO_2 electrodes were immersed in ethanol containing 0.5 mM photosensitizer (**SB1**, **SB2** or **SB3**) for 2 h at 40 °C. Pt counter electrodes were prepared by spreading a droplet of 7 mM H_2PtCl_6 in 2-propanol on top of a FTO substrate and heating heated at 400 °C for 20 min. The two electrodes were sealed with 60 μm thick Surlyn (Solaronix). Redox electrolyte was introduced through a small hole drilled in the counter electrode. The electrolyte employed was a solution of 0.7 M 1-methyl-3-propylimidazolium iodide (MPII), 0.03 M iodine (I_2), 0.10 M lithium iodide (LiI) and 0.5 M 4-*tert*-butylpyridine (TBP) in a mixture of acetonitrile and valeronitrile (volume ratio, 85:15). Photocurrent and voltage were measured from a solar simulator (Oriel Sol 3A class AAA) equipped with 450 W Xenon lamp (Newport 6279NS) and a Keithley 2400 source meter. Light intensity was adjusted with the NREL-calibrated Si solar cell having KG-2 filter for approximating one sun illumination (100 mW/cm^2). The cell was covered with an aperture black mask to measure photocurrent and voltage accurately. The incident photon-to-current conversion efficiency (IPCE) spectra was measured as a function of wavelength from 300 to 800 nm under DC measurement mode using a specially designed IPCE system (PV Measurements, Inc.), where 75 W Xe light source was used for monochromatic light. The absorbance of photosensitizers was recorded by a UV–Vis spectrophotometer (Agilent 8453) in the wavelength range of 300–800 nm. Impedance spectra were recorded using a Autolab (AUT128N, FRA2) electrochemical station under one sun illumination with a frequency range of 0.1 Hz–100 kHz.

2.4. Synthesis of photosensitzres

Compounds **1b**–**7** were prepared according to the modified literature procedures [27–34]. ^{1}H and ^{13}C NMR spectra of all compounds are available in the Supplementary material.

2.4.1. 1,4-Dipropoxybenzene (*1b*)

A suspension of KOH (2.16 g, 0.038 mol) in ethanol (10 mL) was stirred at room temperature. Hydroquinone (2.00 g, 0.018 mol) was added dropwise. 1-Bromohexane (3.8 mL, 0.038 mol) was added to the stirred mixture. After stirring for 24 h with heating at reflux, the ethanol was evaporated at reduced pressure. The residue was then extracted with chloroform. The combined organic layer was washed with water and dried over anhydrous magnesium sulfate. The white solid product **1b** (3.01 g, 0.015 mol) was obtained in 86% yield after column chromatography on silica gel (eluent *n*-Hx:CH_2Cl_2 = 5:1, R_f = 0.50). ^{1}H NMR (300 MHz, $CDCl_3$): δ 6.77 (s, 4H,

Ar), 3.77 (t, J = 6.6 Hz, 4H, CH_2), 1.76–1.70 (m, 4H, CH_2), 0.99 (t, J = 7.5 Hz, 6H, CH_3).

*2.4.2. 1,4-Bis(hexyloxy)benzene (**1c**)*

The synthetic method resembles that of compound **1b**, and compound **1c** was purified by column chromatography on silica gel (eluent *n*-Hx:CH_2Cl_2 = 5:1, R_f = 0.50) to obtain in 88% yield as white solid. ^{1}H NMR (300 MHz, $CDCl_3$): δ 6.82 (s, 4H, Ar), 3.90 (t, J = 6.6 Hz, 4H, CH_2), 1.80–1.73 (m, 4H, CH_2), 1.47–1.30 (m, 12H, CH_2), 0.90 (t, J = 5.7 Hz, 6H, CH_3).

*2.4.3. 1,4-Diiodo-2,5-dimethoxybenzene (**2a**)*

A solution of H_5IO_6 (3.20 g, 0.014 mol) in methanol (25 mL) was stirred for 10 min, and I_2 (6.97 g, 0.028 mol) was added. After the solution was stirred for another 10 min, 1,4-dimethoxybenzene (3.00 g, 0.022 mol) was added and the mixture heated at 70 °C for 4 h. The resulting solution was poured into a solution of $K_2S_2O_5$ (6.20 g, 0.028 mol) in water (50 mL). The precipitate was washed with methanol and dissolved in methylene chloride. After filtration, the filtrate was collected and evaporated under vacuum to afford a white solid (8.12 g, 0.021 mol) in 90% yield. ^{1}H NMR (300 MHz, $CDCl_3$): δ 7.19 (s, 2H, Ar), 3.82 (s, 6H, CH_3).

*2.4.4. 1,4-Diiodo-2,5-dipropoxybenzene (**2b**)*

The synthetic method resembles that of compound **2a**, and compound **2b** was obtained in 92% yield as white solid. ^{1}H NMR (300 MHz, $CDCl_3$): δ 7.17 (s, 2H, Ar), 3.90 (t, J = 6.3 Hz, 4H, CH_2), 1.86–1.79 (m, 4H, CH_2), 0.90 (t, J = 7.2 Hz, 6H, CH_3).

*2.4.5. 1,4-Bis(hexyloxy)-2,5-diiodobenzene (**2c**)*

The synthetic method resembles that of compound **2a**, and compound **2c** was obtained in 90% yield as white solid. ^{1}H NMR (300 MHz, $CDCl_3$): δ 7.17 (s, 2H, Ar), 3.93 (t, J = 6.3 Hz, 4H, CH_2), 1.82–1.75 (m, 4H, CH_2), 1.53–1.32 (m, 12H, CH_2), 0.91 (t, J = 6.6 Hz, 6H, CH_3).

*2.4.6. 4-Iodo-2,5-dimethoxybenzaldehyde (**3a**)*

A solution of compound **2a** (2.00 g, 5.130 mmol) in diethyl ether (60 mL) was cooled to −10 °C. To this solution was added dropwise *n*-BuLi (1.60 M in hexane, 3.20 mL) over 20 min. The reaction mixture was stirred in an ice/brine bath at −8 to −5 °C for 1 h. DMF (0.60 mL, 7.690 mmol) was added in one portion. The reaction mixture was allowed to warm to room temperature over 6 h and then poured into water in a separatory funnel. The organic layer was washed with H_2O and brine once and dried over magnesium sulfate. After removed the solvent under vacuum, the residue was purified by column chromatography on silica gel (eluent *n*-Hx:EA = 8:1, R_f = 0.30) to obtain compound **3a** (1.20 g, 3.591 mmol) in 70% yield as white solid. ^{1}H NMR (300 MHz, $CDCl_3$): δ 10.40 (s, 1H, CHO), 7.47 (s, 1H, Ar), 7.23 (s, 1H, Ar), 3.90 (s, 3H, CH_3), 3.88 (s, 3H, CH_3).

*2.4.7. 4-Iodo-2,5-dipropoxybenzaldehyde (**3b**)*

The synthetic method resembles that of compound **3a**, and compound **3b** was purified by column chromatography on silica gel (eluent *n*-Hx:CH_2Cl_2 = 5:1, R_f = 0.15) to obtain in 62% yield as white solid. ^{1}H NMR (300 MHz, $CDCl_3$): δ 10.42 (s, 1H, CHO), 7.45 (s, 1H, Ar), 7.17 (s, 1H, Ar), 4.00–3.94 (m, 4H, CH_2), 1.90–1.78 (m, 4H, CH_2), 1.06 (t, J = 6.6 Hz, 6H, CH_3).

*2.4.8. 2,5-Bis(hexyloxy)-4-iodobenzaldehyde (**3c**)*

The synthetic method resembles that of compound **3a**, and compound **3c** was purified by column chromatography on silica gel (eluent *n*-Hx:CH_2Cl_2 = 5:1, R_f = 0.15) to obtain in 60% yield as white solid. ^{1}H NMR (300 MHz, $CDCl_3$): δ 10.42 (s, 1H, CHO), 7.45 (s, 1H, Ar), 7.19 (s, 1H, Ar), 4.04–3.98 (m, 4H, CH_2), 1.86–1.77 (m, 4H, CH_2), 1.59–1.44 (m, 4H, CH_2), 1.37–1.34 (m, 8H, CH_2), 0.91 (t, J = 6.9 Hz, 6H, CH_3).

*2.4.9. 1-(Hexyloxy)-4-iodobenzene (**4**)*

To a suspension of 4-iodophenol (5.0 g, 22.7 mmol) and K_2CO_3 (4.4 g, 31.8 mmol) in ethanol (30 mL) was added 1-bromohexane (2.9 mL, 20.4 mmol) at room temperature. After being stirred under reflux for 24 h, the mixture was filtered to remove the solid. The crude product was extracted into methylene chloride, washed with water, and dried over anhydrous magnesium sulfate. After removing solvent under reduced pressure, the residue was purified by column chromatography on silica gel (eluent *n*-Hx:CH_2Cl_2 = 5:1, R_f = 0.50) to obtain compound **4** (6.2 g, 20.4 mmol) in 90% yield as viscous colorless oil. ^{1}H NMR (300 MHz, $CDCl_3$): δ 7.54 (d, J = 8.4 Hz, 2H, Ar), 6.67 (d, J = 8.4 Hz, 2H, Ar), 3.91 (t, J = 6.6 Hz, 2H, CH_2), 1.81–1.55 (m, 2H, CH_2), 1.47–1.25 (m, 6H, CH_2), 0.90 (t, J = 6.6 Hz, 3H, CH_3).

*2.4.10. 4-(Hexyloxy)-N-(4-(hexyloxy)phenyl)-N-phenylaniline (**5**)*

To a stirred solution of compound **4** (5.0 g, 16.4 mmol), cuprous chloride (65 mg, 0.6 mmol), 1,10-phenanthroline (236 m g, 1.312 mmol), potassium hydroxide (1.5 g, 26.2 mmol) in anhydrous toluene (12 mL), aniline (598 μL, 6.6 mmol) was added under argon atmosphere. The reaction mixture was refluxed for 12 h and then water added. The crude product was extracted into dichloromethane, and the organic layer was washed with water and dried over anhydrous magnesium sulfate. After removing solvent under reduced pressure, the residue was purified by column chromatography silica gel (eluent *n*-Hx:CH_2Cl_2 = 1:1, R_f = 0.50) to obtain compound **5** (1.8 g, 4.0 mmol) in 60% yield as viscous yellowish oil. ^{1}H NMR (300 MHz, $CDCl_3$): δ 7.17 (d, J = 7.5 Hz, 2H, Ar), 7.03 (d, J = 9.0 Hz, 4H, Ar), 6.93 (d, J = 9.0 Hz, 2H, Ar), 6.82 (t, J = 7.2 Hz, 1H, Ar), 6.80 (d, J = 9.0 Hz, 2H, Ar), 3.91 (t, J = 6.6 Hz, 4H, CH_2), 1.81–1.55 (m, 4H, CH_2), 1.46–1.45 (m, 4H, CH_2), 1.36–1.31 (m, 8H, CH_2), 0.91 (t, J = 6.9 Hz, 6H, CH_3).

*2.4.11. 4-(Bis(4-(hexyloxy)phenyl)amino)benzaldehyde (**6**)*

To a cold solution of compound **5** (1.50 g, 3.36 mmol) in *N*,*N*-dimethylformamide (15 mL) at 0 °C was added a Vilsmeier reagent, which was prepared by phosphorus oxychloride (345 μL 3.70 mmol) and *N*,*N*-dimethylformamide (5 mL) mixture. The reaction mixture was stirred at room temperature for 48 h and then water added. The crude product was extracted into dichloromethane, washed with water, and dried over anhydrous magnesium sulfate. After removing solvent under reduced pressure, the residue was purified by column chromatography on silica gel (eluent *n*-Hx:EA = 8:1, R_f = 0.33) to obtain compound **6** (1.4 g, 2.86 mmol) in 85% yield as viscous yellowish oil. ^{1}H NMR (300 MHz, $CDCl_3$): δ 9.74 (s, 1 H, CHO), 7.61 (d, J = 9.0 Hz, 2H, Ar), 7-12-7.09 (m, 4H, Ar), 6.90–6.81 (m, 6H, Ar), 3.94 (t, J = 6.6 Hz, 4H, CH_2), 1.80–1.75 (m, 4H, CH_2), 1.48–1.44 (m, 4H, CH_2), 1.36–1.31 (m, 8H, CH_2), 0.91 (t, J = 6.9 Hz, 6H, CH_3).

*2.4.12. 4-(Hexyloxy)-N-(4-(hexyloxy)phenyl)-N-(4-vinylphenyl) aniline (**7**)*

Methyltriphenyl-phosphonium bromide (634 mg, 1.774 mmol) and compound **6** (700 mg, 1.478 mmol) were dissolved in 10 mL of anhydrous THF under argon. A solution of potassium *tert*-butoxide (1.0 M THF; 2.2 mL, 2.217 mmol) was slowly dropwised to the resulting mixture at room temperature. The mixture was stirred for 8 h and then water added. The crude product was extracted into dichloromethane, washed with water, and dried over anhydrous magnesium sulfate. After removing solvent under reduced pressure, the residue was purified by column chromatography on silica

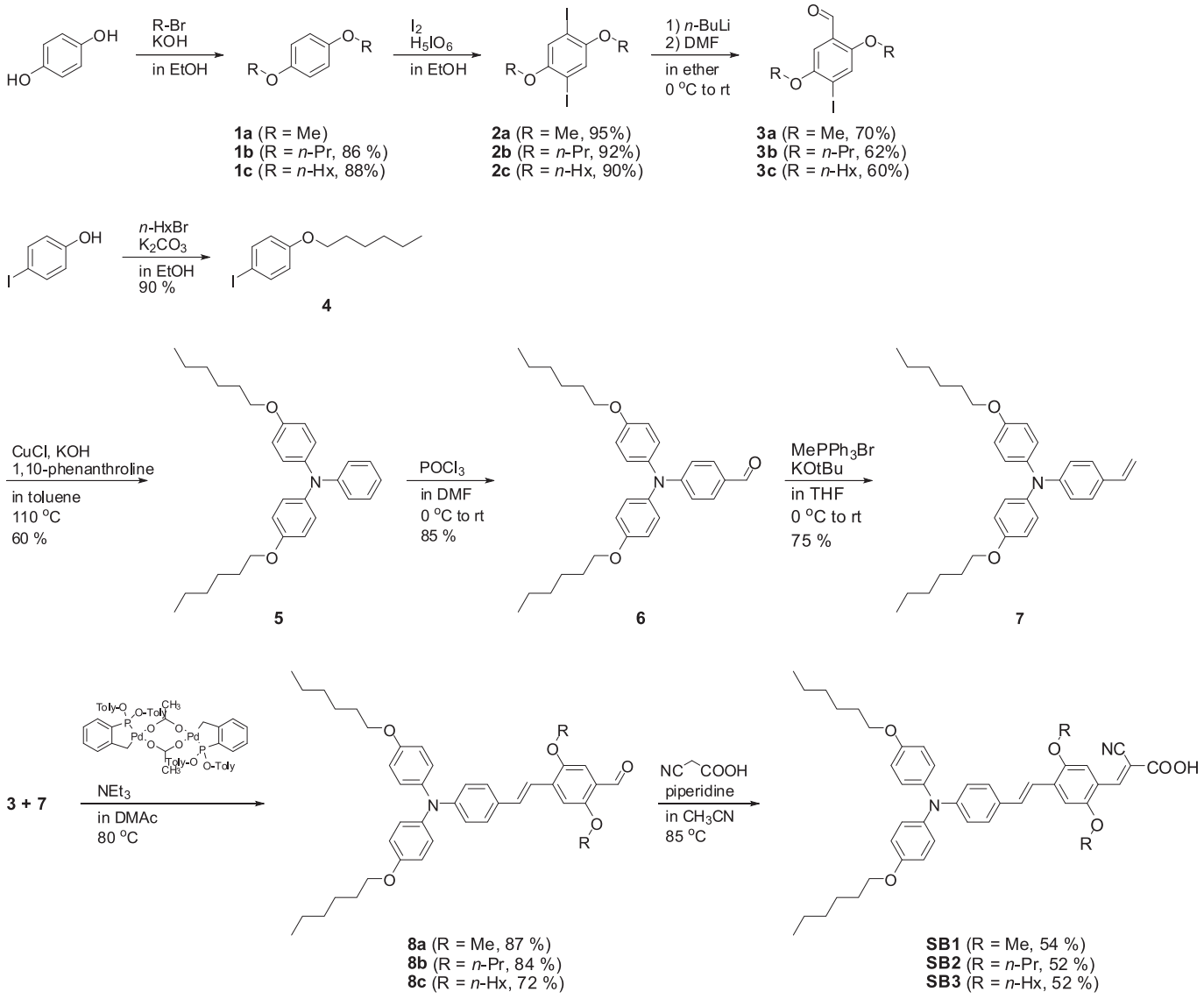

Scheme 1. Synthetic procedure of organic dyes **SB1**, **SB2**, and **SB3**.

gel (eluent *n*-Hx:CH_2Cl_2 = 5:1, R_f = 0.27) to obtain compound **7** (523 mg, 1.109 mmol) in 75% yield as viscous yellowish oil. ^{1}H NMR (300 MHz, $CDCl_3$): δ 7.17 (d, J = 9.0 Hz, 2H, Ar), 7.00 (d, J = 9.0 Hz, 4H, Ar), 6.85 (d, J = 8.7 Hz, 2H, Ar), 6.77 (d, J = 8.7 Hz, 2H, Ar), 6.58 (dd, J = 17.4 Hz, 1H, CH), 5.53 (d, J = 17.7 Hz, 1H, CH=CH_2), 5.04 (d, J = 10.8 Hz, 1H, CH=CH_2), 1.79–1.70 (m, 4H, CH_2), 1.49–1.40 (m, 4H, CH_2), 1.35–1.30 (m, 8H, CH_2), 0.88 (t, J = 6.9 Hz, 6H, CH_3). ^{13}C NMR (75 MHz, $CDCl_3$): δ 155.5, 148.6, 140.7, 136.4, 129.9, 126.9, 126.6, 126.4, 120.4, 115.3, 111.0, 68.2, 31.7, 29.8, 29.4, 25.9, 22.7, 14.2. ESI-HRMS (positive) calcd for $[C_{32}H_{42}NO_2]^+$ 472.3216 found 472.3170.

2.4.13. 4-(4-(Bis(4-(hexyloxy)phenyl)amino)styryl)-2,5-dimethoxybenzaldehyde (*8a*)

Trimethylamine (286 ml, 2.055 mmol) was added to a solution of compound **7** (775 mg 1.63 mmol), aldehyde **3a** (400 mg, 1.370 mmol) and *trans*-di(*μ*-aceto)bis[*o*-(di-*o*-tolyphosphino) benzyl]-dipalladium(II) (30 mg, 0.032 mmol) in 5 mL of *N*,*N*-dimethylacetamide, DMAc under argon atmosphere. The resulting mixture was stirred at 80 °C for 72 h. The reaction mixture was cooled to room temperature and then saturated sodium chloride aqueous solution added. The crude product was extracted into methylene chloride, washed with water, and dried over anhydrous magnesium sulfate. After removing solvent under reduced pressure, the residue was purified by column chromatography on silica gel (eluent *n*-Hx:EA = 8:1, R_f = 0.23) to obtain compound **8a** (732 mg, 1.151 mmol) in 84% yield as viscous orange oil. ^{1}H NMR (300 MHz, $CDCl_3$): δ 10.40 (s, 1 H, CHO), 7.37–6.80 (m, 16H, Ar), 3.95–3.90 (m, 7H, CH_2 and CH_3), 3.86 (s, 3H, CH_3), 1.79–1.72 (m, 4H, CH_2), 1.49–1.44 (m, 4H, CH_2), 1.36–1.31 (m, 8H, CH_2), 0.91 (t, J = 6.9 Hz, 6H, CH_3). ^{13}C NMR (75 MHz, $CDCl_3$): δ 188.9, 156.9, 155.9, 151.2, 149.2, 140.4, 135.1, 132.4, 129.1, 127.9, 127.0, 123.6, 112.0, 119.6, 115.4, 109.3, 109.0, 68.4, 56.3, 56.2, 31.7, 29.4, 25.9, 22.7, 14.1. ESI-HRMS (positive) calcd for $[C_{41}H_{50}NO_5]^+$ 635.3689 found 635.4802.

2.4.14. 4-(4-(Bis(4-(hexyloxy)phenyl)amino)styryl)-2,5-dipropoxybenzaldehyde (*8b*)

The synthetic method resembles that of compound **8a**, and compound **8b** was purified by column chromatography on silica gel (eluent *n*-Hx:EA = 15:1, R_f = 0.23) to obtain in 84% yield as viscous orange oil. ^{1}H NMR (300 MHz, $CDCl_3$): δ 10.43 (s, 1 H, CHO), 7.35–6.81 (m, 16H, Ar), 4.05 (t, J = 6.6 Hz, 2H, CH_2), 4.03–3.90 (m, 6H, CH_2), 1.90–1.72 (m, 8H, CH_2), 1.46–1.41 (m, 4H, CH_2),

1.36–1.34 (m, 8H, CH_2), 1.10–1.05 (m, 6H, CH_2), 0.91 (t, J = 6.6 Hz, 6H, CH_3). ^{13}C NMR (75 MHz, $CDCl_3$): δ 189.0, 156.5, 155.9, 150.6, 149.1, 140.4, 135.2, 132.2, 129.2, 127.8, 127.0, 123.8, 119.9, 115.4, 110.2, 110.1, 70.8, 70.7, 68.4, 31.7, 29.8, 29.4, 25.9, 22.8, 22.7, 14.1, 10.8, 10.7. ESI-HRMS (positive) calcd for $[C_{45}H_{58}NO_5]^+$ 692.4315, found 692.4310.

*2.4.15. 4-(4-(Bis(4-(hexyloxy)phenyl)amino)styryl)-2,5-bis(hexyloxy)benzaldehyde (**8c**)*

The synthetic method resembles that of compound **8a**, and compound **8c** was purified by column chromatography on silica gel (eluent *n*-Hx : EA = 15:1, R_f = 0.33) to obtain in 72% yield as viscous orange oil. ^{1}H NMR (300 MHz, $CDCl_3$): δ 10.42 (s, 1 H, CHO), 7.35–6.80 (m, 16H, Ar), 4.07 (t, J = 6.6 Hz, 2H, CH_2), 3.98 (t, J = 6.0 Hz, 2H, CH_2), 3.91 (t, J = 6.6 Hz, 4H, CH_2), 1.85–1.71 (m, 8H, CH_2), 1.48–1.41 (m, 8H, CH_2), 1.35–1.33 (m, 16H, CH_2), 0.93–0.89 (m, 12H, CH_2 and CH_3). ^{13}C NMR (75 MHz, $CDCl_3$): δ 188.9, 156.4, 155.9, 150.6, 149.1, 140.3, 135.1, 132.1, 129.1, 127.7, 126.9, 123.8, 119.9, 115.4, 110.1, 110.0, 69.2, 69.1, 68.3, 31.7, 31.6, 29.3, 25.9, 25.8, 22.7, 14.1. ESI-HRMS (positive) calcd for $[C_{51}H_{70}NO_5]^+$ 776.5254, found 776.5209.

*2.4.16. 4-(Bis(4-(hexyloxy)phenyl)amino)styryl)-2,5-dimethoxyphenyl)-2-cyanoacrylic acid (**SB1**)*

A mixture of compound 8a (240 mg, 0.377 mmol) and cyanoacetic acid (42 mg, 0.490 mmol) was vacuum dried, and acetonitrile (40 mL) and piperidine (37 μL, 0.377 mmol) were added under argon atmosphere. The reaction mixture was refluxed for 10 h. The reaction mixture was cooled to room temperature and then saturated sodium chloride aqueous solution added. The crude product was extracted into methylene chloride, washed with water, and dried over anhydrous magnesium sulfate. After removing solvent under reduced pressure, the residue was purified by column chromatography on silica gel (eluent CH_2Cl_2:MeOH = 10:1, R_f = 0.13) to obtain compound **SB1** (138 mg, 0.196 mmol) in 54% yield as red solid. ^{1}H NMR (300 MHz, $CDCl_3$): δ 8.68 (s, 1 H, CH), 7.96 (s, 1H, CH), 7.33–6.79 (m, 15H, Ar), 3.95–3.91 (m, 10H, CH_2 and CH_3), 1.80–1.75 (m, 4H, CH_2), 1.48–1.44 (m, 4H, CH_2), 1.36–1.28 (m, 8H, CH_2), 0.91 (t, J = 6.9 Hz, 6H, CH_3). ^{13}C NMR (75 MHz, $CDCl_3$): δ 168.9, 155.9, 154.9, 149.2, 140.6, 140.2, 135.6, 132.9, 128.7, 128.1, 127.1, 126.8, 119.6, 118.9, 116.6, 115.4, 110.3, 107.7, 68.4, 56.3, 56.1, 31.7, 29.8, 29.4, 25.9, 22.7, 14.2. ESI-HRMS (positive) calcd for $[C_{44}H_{50}N_2O_6]^+$ 703.3747 found 703.3702.

*2.4.17. 4-(Bis(4-(hexyloxy)phenyl)amino)styryl)-2,5-dipropoxyphenyl)-2-cyanoacrylic acid (**SB2**)*

The synthetic method resembles that of compound **SB1**, and compound **SB2** was purified by column chromatography on silica gel (eluent CH_2Cl_2:MeOH = 5:1, R_f = 0.33) to obtain in 52% yield as red solid. ^{1}H NMR (300 MHz, $CDCl_3$): δ 8.59 (s, 1 H, CH), 7.73 (s, 1H, CH), 7.23–6.78 (m, 15H, Ar), 3.91 (t, J = 5.3 Hz, 8H, CH_2), 1.80–1.73 (m, 8H, CH_2), 1.48–1.42 (m, 4H, CH_2), 1.37–1.27 (m, 8H, CH_2), 0.92 (t, J = 6.6 Hz, 12H, CH_3). ^{13}C NMR (75 MHz, $CDCl_3$): δ 164.8, 155.7, 153.4, 150.1, 148.6, 140.5, 137.5, 133.1, 131.0, 129.6, 127.8, 126.8, 120.1, 115.3, 110.3, 109.0, 70.9, 70.3, 68.3, 31.7, 29.8, 29.5, 26.0, 22.7, 14.2, 10.9, 10.6. ESI-HRMS (positive) calcd for $[C_{48}H_{59}N_2O_6]^+$ 759.4373 found 759.4328.

*2.4.18. 4-(Bis(4-(hexyloxy)phenyl)amino)styryl)-2,5-bis(hexyloxy)phenyl)-2-cyanoacrylic acid (**SB3**)*

The synthetic method resembles that of compound **SB1**, and compound **SB3** was purified by column chromatography on silica gel (eluent CH_2Cl_2:MeOH = 5:1, R_f = 0.60) to obtain in 52% yield as red solid. ^{1}H NMR (300 MHz, $CDCl_3$): δ 8.63 (s, 1 H, CH), 7.74 (s, 1H, CH), 7.25–6.79 (m, 15H, Ar), 3.92 (t, J = 6.3 Hz, 8H, CH_2), 1.80–1.75 (m, 8H, CH_2), 1.46–1.26 (m, 28H, CH_2), 0.92 (m, 12H, CH_3). ^{13}C NMR (75 MHz, $CDCl_3$): δ 168.2, 155.8, 153.5, 150.2, 148.8, 140.6, 133.4, 129.2, 115.4, 111.4, 109.6, 69.5, 69.0, 68.4, 31.9, 31.8, 31.6, 29.8, 29.5, 29.0, 26.2, 25.9, 25.6, 22.7, 14.2. ESI-HRMS (positive) calcd for $[C_{54}H_{71}N_2O_6]^+$ 843.5312 found 843.5335.

3. Results and discussion

SB1, **SB2**, and **SB3** were synthesized by the stepwise synthetic procedure (Scheme 1). First, compounds of **3a**–**3b** such as dialkyloxy substituted *p*-phenylenevinylene spacer were prepared in three steps from *p*-hydroquinone [27]. A Williamson etherification of *p*-hydroquinone [28] followed by iodination [29] gave **2a**–**2c**. Monolithiation of **2a**–**2c** and quenching the aryllithium by using anhydrous DMF obtained dialkyloxy substituted benzaldehyde **3a**–**3c**. 1-Bromo-4-hexyloxybenzene **4** was prepared from 4-iodophenol [30]. After that, 4-(hexyloxy)-*N*-(4-(hexyloxy)phenyl)-*N*-phenylaniline **5** was obtained from the reaction of aniline with compound **4** *via* the Ullmann condensation [31]. Compound **5** was converted into its corresponding 4-(bis(4-(hexyloxy)phenyl) amino)-benzaldehyde **6** by means of the Vilsmeier–Haack reaction [32]. 4-(Hexyloxy)-*N*-(4-(hexyloxy)phenyl)-*N*-(4-vinylphenyl) aniline **7** was prepared from the reaction of compound **6** with methyltriphenyl-phosphonium bromide [20f]. Coupling reaction of aldehydes **3a**–**3c** with compound **7** under the Heck reaction led to its corresponding aldehydes **8a**–**8c** in good yields (72–87%) [33]. The aldehydes **8a**–**8c**, upon reaction with cyanoacetic acid in the presence of piperidine as base *via* the Knoevenagel condensation, produced **SB1**, **SB2** and **SB3** in moderate yields (52–54%).

UV–Vis absorption and emission spectra of **SB1**, **SB2**, and **SB3** in ethanol are shown in Fig. 2 and their absorption data are listed in Table 1. In UV–Vis spectra, the absorption of **SB1** ~ **SB3** exhibits two major bands at 305–306 nm and at 447–448 nm. The former is attributed to a localized aromatic π–π* transitions and the later is ascribed to charge-transfer (CT) transitions. The absorption coefficient (ε) at absorption maximum of **SB1**, **SB2** and **SB3** in ethanol is 33,637 M^{-1} cm^{-1} at 447 nm, 29,703 M^{-1} cm^{-1} at 448 nm and 40,922 M^{-1} cm^{-1} at 448 nm, respectively. Structural difference

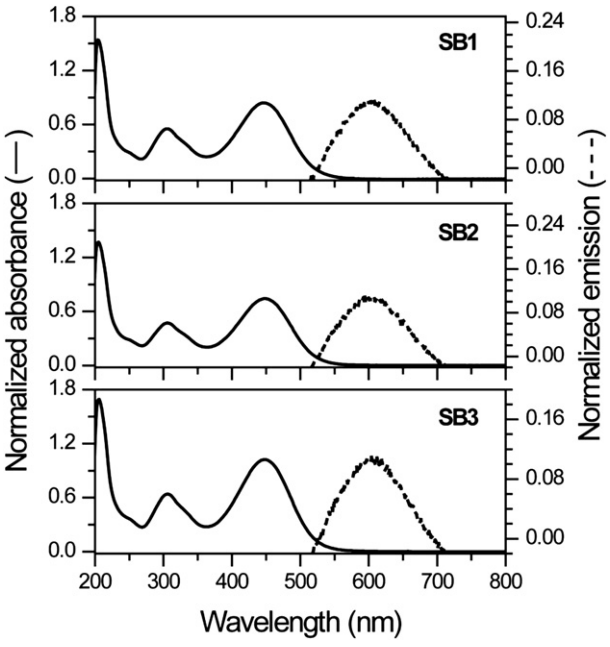

Fig. 2. Absorption and emission spectra of **SB1**, **SB2** and **SB3** dyes in ethanol.

Table 1
Absorption and electrochemical properties of **SB1**, **SB2** and **SB3** dyes.

Dye	λ_{max} (nm)[a]	ε (M^{-1} cm^{-1}) [a]	λ_{max} (nm) [a]	ε (M^{-1} cm^{-1}) [a]	E_{HOMO} (V) [b]	E_{0-0} (V) [c]	E_{red} (V) [d]
SB1	305	22,119	447	33,637	1.23	2.27	−1.04
SB2	306	18,878	448	29,703	1.19	2.27	−1.08
SB3	306	25,611	448	40,922	1.14	2.25	−1.11

[a] Absorption spectra were measured in ethanol solution.
[b] E_{HOMO} was calculated by $E_{red} - E_{0-0}$.
[c] E_{0-0} was determined from intersection of absorption and emission spectra.
[d] E_{red} were measured in CH_2Cl_2 with 0.1 M $(Bu_4N)PF_6$ at scan rate of 100 mV s^{-1}.

between the previously reported **TA-St-CA** and **TA-DM-CA** dyes [22] and the **SB**-series dyes is that the **SB**-series dyes have two hexyloxy groups attached to the triphenylamine on the electron donor moiety as well as two alklyoxy groups in *p*-phenylenevinylene spacer unit. These substituted alkyloxy groups enhance the extent of electron delocalization over the whole molecule, so their maximum absorption peaks are red shifted by about 60 nm and 15 nm than that of **TA-St-CA** and **TA-DM-CA**. **SB1**, **SB2**, and **SB3** show luminescence maxima at 604 nm, 596 nm, and 606 nm when they are excited within their $\pi-\pi^*$ band at 298 K.

With respect to the conduction band edge of TiO_2 and the redox potential of electrolyte, proper energy levels of lowest unoccupied molecular orbital (LUMO) and highest occupied molecular orbital (HOMO) of dyes are required to separate electrons from LUMO and holes from HOMO. Fig. 3 shows the cyclic voltammograms of **SB1**, **SB2** and **SB3** dyes in the potential range of 2.0 to −2.0 V. In the negative potential region, the reduction potential (E_{red}) of **SB1** exhibits a quasi-reversible behavior at −1.04 V, which corresponds to LUMO energy level. Under the same conditions, LUMO energy levels of **SB2** and **SB3** are determined to be −1.08 V and −1.11 V, respectively. These levels are higher than the conduction band edge energy level (−0.74 V *vs.* SCE) [2c] of the TiO_2, so electron injection is expected from LUMO to the conduction band of TiO_2. The HOMO levels are calculated from E_{red} and E_{0-0} determined by the intersection of absorption and emission spectra listed in Table 1. The HOMO values of **SB1**, **SB2**, and **SB3** are determined to be 1.23 V, 1.19 V, and 1.14 V *vs.* SCE. As depicted in Fig. 4, these levels are more positive than the I^-/I_3^- redox potential (0.20 V *vs.* SCE) [34] so that the oxidized dyes can be thermodynamically accept electrons from I^- ion in iodide/triiodide electrolyte for regeneration.

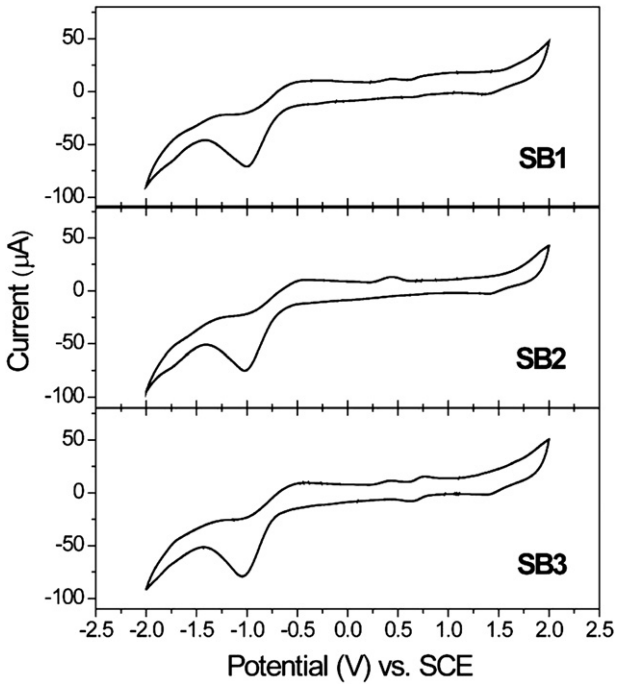

Fig. 3. Cyclic voltammograms of **SB1**, **SB2**, and **SB3** measured in CH_2Cl_2 solution containing 0.1 M $(Bu_4N)PF_6$ at scan rate of 100 mV s^{-1}. Pt and saturated calomel electrode (SCE) were used as the counter electrode and as the reference electrode, respectively.

To understand the electron distribution at ground and excited states in **SB**-series dyes, the electronic property of **SB1**, **SB2** and **SB3** are studied *via* density functional theory (DFT). The computational calculations were performed using Gaussian09 software package [35]. The DFT was applied B3LYP exchange-correlation functional [36] and 6-31G(d) basis set [37]. Fig. 5 shows the resulting electron distributions of **SB1**, **SB2** and **SB3**. Molecular orbital calculations on the **SB1**-**SB3** indicated that electrons in the HOMO levels spread over the π-framework from 4-(hexyloxy)-*N*-(4-(hexyloxy)phenyl)-*N*-phenylaniline to *p*-phenylenevinylene spacers. At the LUMO levels excited electrons are shifted from the electron donating 4-(hexyloxy)-*N*-(4-(hexyloxy)phenyl)-*N*-phenylaniline units to the electron accepting cyanoacrylic acid unit due to the intramolecular charge transfer along the π-conjugated skeleton. Therefore, we can expect that the spatial orientation of HOMO and LUMO levels for the dyes is suitable for DSSCs, which can facilitate the interfacial electron injection from the excited dye to the conduction band of TiO_2.

The photovoltaic performance of **SB1**, **SB2** and **SB3** is evaluated by employing a thin (5.0 μm) transparent TiO_2 film and a redox electrolyte of 0.7 M MPII, 0.03 M I_2, 0.10 M LiI and 0.5 M TBP in a mixture of acetonitrile and valeronitrile (volume ratio, 85:15), which is compared with that of conventional ruthenium complex dye coded **N719** and **TA-DM-CA**. Fig. 6 shows photocurrent density−voltage curves of **SB1**, **SB2**, **SB3** and **N719** along with **TA-DM-CA**.

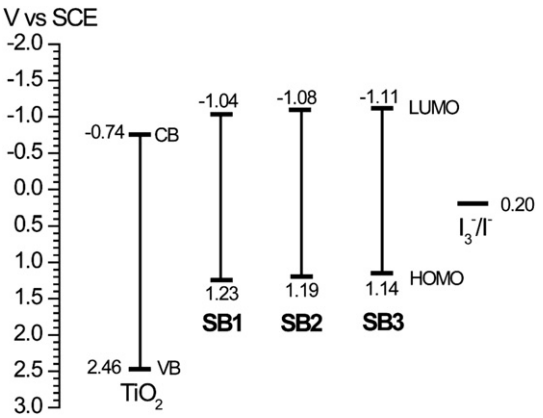

Fig. 4. LUMO and HOMO energy levels of **SB1**, **SB2** and **SB3** dyes with respect to the conduction band (CB) edge and the valence band (VB) edge energies of TiO_2 and the I_3^-/I^- redox potential.

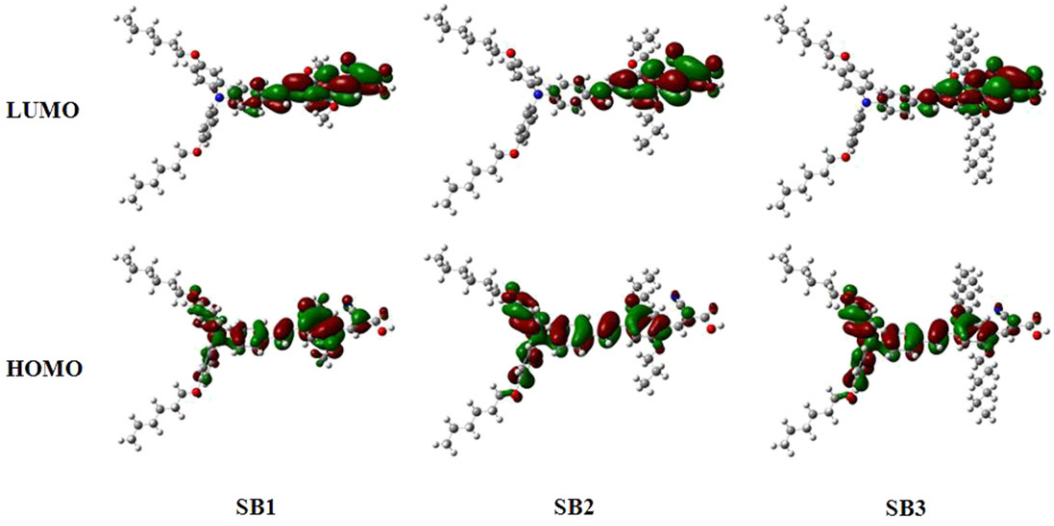

Fig. 5. Frontier molecular orbitals of **SB1**, **SB2** and **SB3**.

The photovoltaic characteristic parameters of J_{SC}, V_{OC}, *FF* and η are summarized in Table 2. Under standard AM 1.5G 1 sun (100 mW/cm^2) illumination condition, V_{OC} increases from 0.706 V (**SB1**) to 0.731 V (**SB2**) and to 0.757 V (**SB3**), while little change in J_{SC} (11.07 mA/cm^2 for **SB1**, 10.71 mA/cm^2 for **SB2** and 10.90 mA/cm^2 for **SB3**) is observed. Due to the increased V_{OC}, the overall conversion efficiency increases from 4.76% (**SB1**) to 4.83% (**SB2**) and to 5.21% (**SB3**). Compared to the **SB** series, the efficiency of **N719** is slightly higher due to slightly higher V_{OC} and *FF*. For the case of **TA-DM-CA**, J_{SC} of 9.37 mA/cm^2 is lower than those of the alkyloxy substituted **SB** series, which is due to larger HOMO–LUMO gap energy, associated with shorter absorption wavelength (see IPCE in Fig. 7). It is noted that V_{OC} increases from 0.706 V to 0.757 V as the substituted alkyloxy chain length increase from methyl to hexyl and V_{OC} of **SB3** is close to that of **N719**. The enhancement of V_{OC} are probably due to reduced recombination ability at TiO_2/electrolyte interface by substitution of insulating alkyloxy chains on the dyes, which will be discussed in detail with impedance spectra. Fig. 7 shows IPCE spectra for the DSSCs sensitized with **SB1**, **SB2** and **SB3** and those are compared with that of **N719** and **TA-DM-CA**-sensitized DSSC. The **SB1**, **SB2** and **SB3** dyes show higher IPCE in the region from 350 nm to 600 nm than **N719**. The IPCE maximum values reach 78% at around 480 nm for all three organic dyes, while **N719** has maximum IPCE of about 70% at 540 nm. The **SB1** sensitizer shows slightly higher IPCE at wavelength ranging from 550 to 700 nm than **SB2** and **SB3**, which is responsible for slightly higher J_{SC}. Although IPCE of **N719** is lower than those of **SB** series in the wavelength ranging from 350 nm to 600 nm, its J_{SC} is similar to those of **SB** dyes due to higher IPCE in the wavelength region from 600 nm to 750 nm.

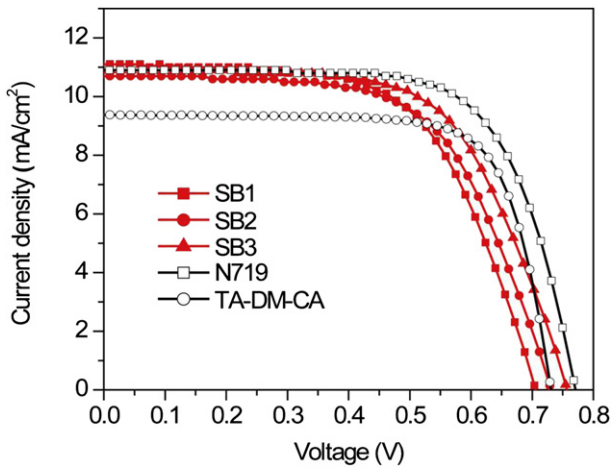

Fig. 6. Photocurrent density–voltage characteristics of the DSSCs based on **SB1**, **SB2**, **SB3 N719** and **TA-DM-CA**. TiO_2 film thickness was 5.0 μm. Measurements were performed under AM 1.5 G 1sun light illumination (100 mW/cm^2) and the cells were covered with aperture masks during measurement. Electrolyte used was composed of 0.7 M 1-methyl-3-propylimidazolium iodide (MPII), 0.03 M iodine (I_2), 0.10 M lithium iodide (LiI) and 0.5 M 4-*tert*-butylpyridine (TBP) in a mixture of acetonitrile and valeronitrile (volume ratio, 85:15).

Electrochemical impedance spectroscopy (EIS) analysis was performed to elucidate the correlation between V_{OC} and the interfacial charge-transfer kinetics. Fig. 8 shows impedance spectra of **SB1**, **SB2**, and **SB3**-sensitized solar cells measured under one sun illumination at open-circuit condition. Typical Nyquist diagram of DSSC is known to be composed of three semicircles for angular frequency (ω) in the impedance function: the first small semicircle (ω_1: higher than 10^3 Hz) is attributed to charge transfer at the Pt/electrolyte interface, the second large semicircle (ω_2: around 10 Hz) to charge transfer at the TiO_2/dye/electrolyte interface, and the third small semicircle (ω_3: around 0.1 Hz) to the carrier transport by ions within the electrolyte [38]. As shown in Fig. 8, little difference is observed in the small ω_1 semicircles, which is due to the fact that the same Pt and electrolyte are used.

Table 2
Open-circuit voltage (V_{OC}), short-circuit photocurrent density (J_{SC}), fill factor (*FF*) and efficiency (η) of the DSSCs[a] based on **SB1**, **SB2**, **SB3**, **N719** and **TA-DM-CA**.

Dye	V_{OC} (V)	J_{SC} (mA/cm^2)	FF	η (%)
SB1	0.706	11.07	0.61	4.76
SB2	0.731	10.71	0.62	4.83
SB3	0.757	10.90	0.63	5.21
N719	0.771	10.89	0.69	5.79
TA-DM-CA	0.730	9.37	0.75	5.10

[a] Active area was 0.45 cm^2. An aperture black mask was used during measurement at AM 1.5G 1 sun light illumination (100 mA/cm^2). TiO_2 film thickness was 5.0 μm. Electrolyte used was composed of 0.7 M 1-methyl-3-propylimidazolium iodide (MPII), 0.03 M iodine (I_2), 0.10 M lithium iodide (LiI) and 0.5 M 4-*tert*-butylpyridine (TBP) in a mixture of acetonitrile and valeronitrile (volume ratio, 85:15).

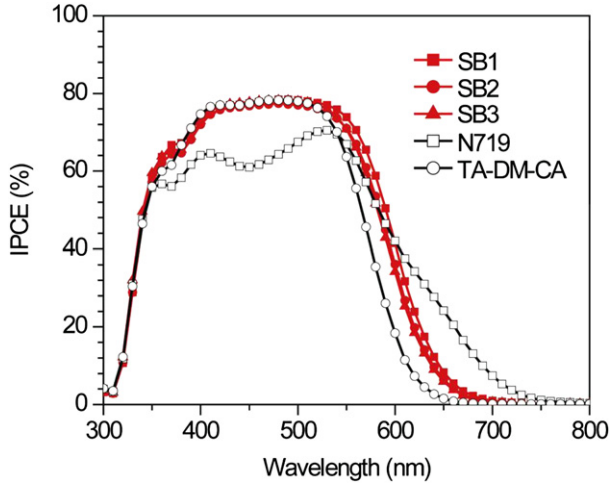

Fig. 7. Incident photon-to-current conversion efficiency (IPCE) as a function of wavelength for the DSSCs based on **SB1**, **SB2**, **SB3 N719** and **TA-DM-CA**. TiO_2 film thickness was 5.0 μm.

On the other hand, there is substantial difference in the large ω_2 semicircles, which indicates that charge-transfer behavior between TiO_2 and electrolyte is significantly altered and this is likely to be due to surface modification with different dyes. The resistances at the TiO_2/electrolyte interface (R_r) are obtained by fit

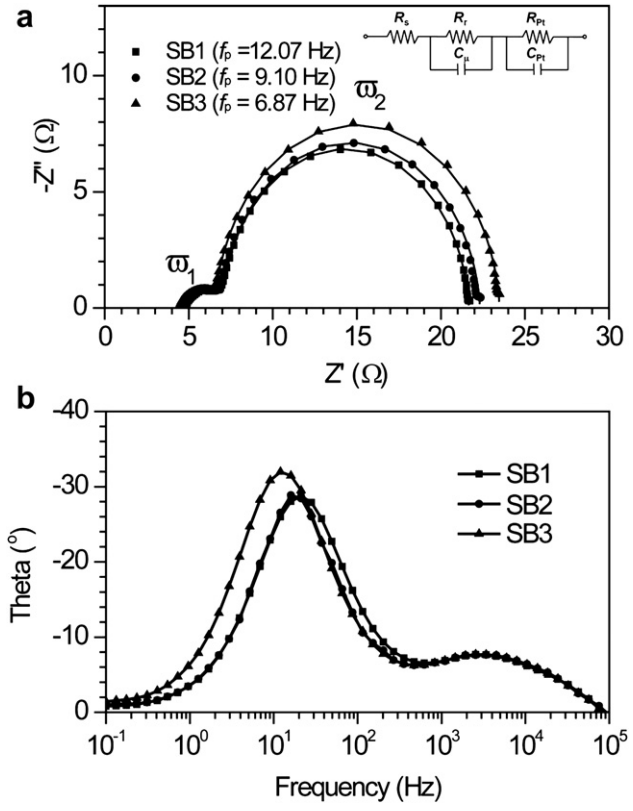

Fig. 8. (a) Nyquist plots and (b) Bode phase plots for the DSSCs based on **SB1** (■), **SB2** (●), and **SB3** (▲) measured under one sun illumination. TiO_2 film thickness for impedance study was 5.0 μm. The inset in (a) shows an equivalent circuit for fitting (–). R_s is the series resistance, R_r is the charge-transfer resistance at the TiO_2/electrolyte interface, C_μ is a constant phase element representing the chemical capacitance, R_{Pt} is the charge-transfer resistance at the counter electrode/electrolyte interface, C_{Pt} is the interfacial capacitance at the counter electrode/electrolyte interface.

Table 3
Electrochemical impedance data for DSSCs based on **SB1**, **SB2** and **SB3**.[a]

Sensitizer	R_r (Ω)	f_p (Hz)	τ_r (ms)[b]
SB1	14.6	12.07	13.19
SB2	15.3	9.10	17.49
SB3	16.8	6.87	23.17

[a] Impedance was measured under one sun illumination with a frequency range of 0.1 Hz–100 kHz at open-circuit voltage. TiO_2 film thickness for impedance study was 5.0 μm.
[b] τ_r was calculated by $1/2\pi f_p$. R_r, f_p and τ_r denote the charge-transfer resistance at the TiO_2/electrolyte interface, the peak frequency at the maximum imaginary resistance of the ω_2: and the time constant for recombination, respectively.

Table 4
Photovoltaic performance of DSSCs based on the **SB1**–**SB3**.[a]

Sensitizer	V_{OC} (V)	J_{SC} (mA/cm^2)	*FF*	η (%)
SB1	0.707	12.62	0.61	5.43
SB2	0.714	13.22	0.64	6.02
SB3	0.745	12.83	0.64	6.12
N719	0.724	15.74	0.67	7.60
TA-DM-CA	0.707	10.96	0.73	5.65

[a] Performance of DSSCs with 0.45 cm^2 working area were obtained under AM 1.5 G 1 sun light illumination (100 mA/cm^2). A black aperture mask was used during measurement. Double-layer TiO_2 film with thickness of 11.5 μm was used. Electrolyte used was composed of 0.7 M MPII, 0.03 M I_2, 0.10 M LiI, and 0.5 M TBP in a mixture of acetonitrile and valeronitrile (volume ratio, 85:15).

the measured data to the equivalent circuit and the time constants for recombination (τ_r) are evaluated using the peak frequency (f_p) data at the maximum imaginary resistance of the ω_2, which are listed in Table 3. R_r increases from **SB1** (14.6 Ω), **SB2** (15.3 Ω) to **SB3** (16.8 Ω), which indicates that charges are not readily transferred from TiO_2 to electrolyte as alkyloxy chain length increases. The f_p value decreases in the order **SB1** (12.07 Hz) > **SB2** (9.10 Hz) > **SB3** (6.87 Hz), which implies that time for recombination increases in the same order because τ_r is inversely proportional to f_p. The τ_r values of **SB1**, **SB2** and **SB3** are determined to be 13.19 ms, 17.49 ms and 23.17 ms from the relation $\tau_r = 1/2\pi f_p$ [39], which can explain the gradual increase in V_{OC} going from **SB1** to **SB3**. As shown in Fig. 8b, the differences in the maximum frequency, associated with lifetime, of **SB** series sensitized DSSCs are

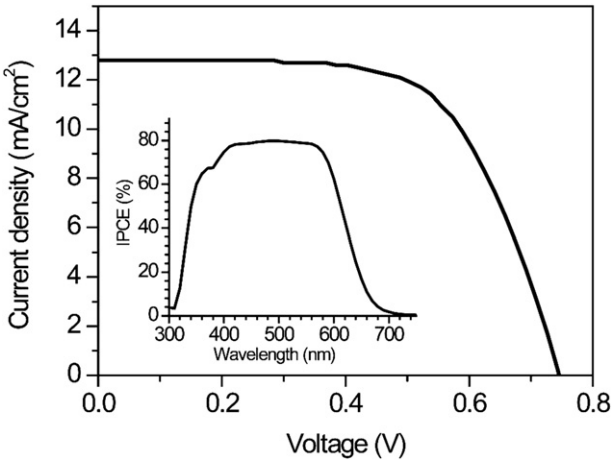

Fig. 9. Photocurrent density–voltage characteristics of DSSCs based on **SB3**. TiO_2 film thickness was 11.5 μm. The inset shows the IPCE spectra of the DSSCs as a function of the wavelength of the light. Measurements were performed under AM 1.5 G light illumination (100 mW/cm^2) and the cells were covered with aperture black masks during measurement. Electrolyte: 0.7 M MPII, 0.03 M I_2, 0.10 M LiI, and 0.5 M TBP in a mixture of acetonitrile and valeronitrile (volume ratio, 85:15).

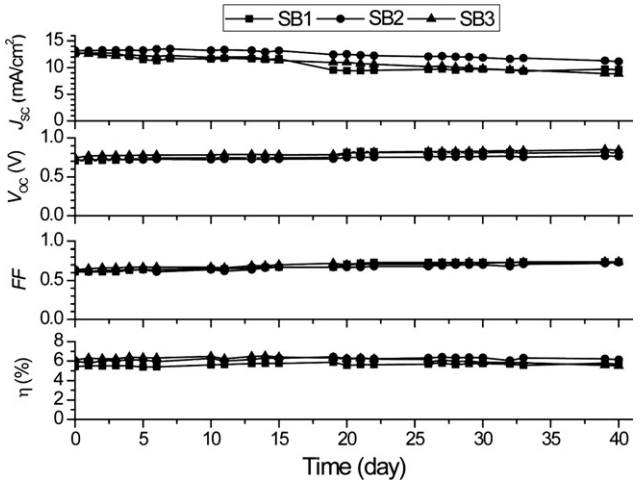

Fig. 10. Variation of photovoltaic parameters (J_{SC}, V_{OC}, *FF* and η) with aging time for the devices sensitized with **SB1**, **SB2** and **SB3**. A double-layer TiO_2 film was employed and an electrolyte used was composed of 0.7 M MPII, 0.03 M I_2, 0.10 M LiI, and 0.5 M TBP in a mixture of acetonitrile and valeronitrile (volume ratio, 85:15).

observed in the Bode phase plots. The frequency peak of the DSSC based on **SB3** is lower than those of the DSSCs based on **SB1** and **SB2**, indicating a longer electron lifetime for **SB3**. It can be said that long alkyloxy chain in **SB**-series dyes is beneficial for prevention of charge recombination.

To improve the photovoltaic performance, we further employ a high quality of double-layer film (11.5 μm) having a light scattering overlayer composed of 500 nm-sized rutile TiO_2 particle [40] to fabricate a high efficient DSSCs based on **SB1**, **SB2** and **SB3**. The photovoltaic characteristic parameters are summarized in Table 4. Compared to the photovoltaic performance from the 5 μm-thick TiO_2 layer in Table 2, the light scattering overlayer contained TiO_2 film improves J_{SC} by about 14–23% without deterioration of V_{OC}. As a result, the conversion efficiency increases from 4.76% to 5.43% for **SB1**, from 4.83% to 6.02% for **SB2** and from 5.21% to 6.12% for **SB3**. In Fig. 9, photocurrent-voltage curve of the **SB3**-sensitized DSSC with double-layer TiO_2 film is depicted along with IPCE.

The stability of the synthesized organic dyes was investigated, where the cells were stored in the dark during long-term stability test. Fig. 10 shows change in the photovoltaic performance as a function of time for 40 days. After 40 days, J_{SC}s decrease slightly, which is probably due to dye desorption from TiO_2 film during illumination [41], but the loss is compensated by the increase in V_{OC} and *FF*. Compared to the initial J_{SC}, it decreases by about 24%, 16% and 32% for **SB1**, **SB2** and **SB3**, respectively. However, V_{OC} increases by about 14%, 7%, 13%, together with increase in *FF* by about 21%, 14% and 16%, which results in almost constant η.

4. Conclusion

We designed and synthesized three organic dyes, namely **SB1**, **SB2**, and **SB3**, which contain different alkyloxy (methyloxy, propyloxy, and hexyloxy) substituted *p*-phenylenevinylene moieties as a π-conjugated spacer. The longer alklyoxy chain substitution was found to be an effective strategy for prevention of electron leakage from nanocrystalline TiO_2 to redox electrolyte, which led to suppression of charge recombination ability and thereby high V_{OC}. Long-term stability test confirmed that the synthesized **SB**-series dyes were quite stable. An optimized **SB3**-sensitized cell using a double-layer TiO_2 film with a light scattering overlayer yielded up to 6.12%.

Acknowledgment

This work was supported by the National Research Foundation of Korea (NRF) grant funded by the Ministry of Education, Science and Technology (MEST) of Korea under contracts No. 2011-0016441, 2010-0028821, 2011-0001055 (ERC program) and R31-2008-10029 (WCU program) and the Korea Institute of Energy Technology Evaluation and planning (KETEP) grant funded by the Ministry of Knowledge Economy under contract No. 20103020010010.

Appendix. Supplementary material

Supplementary data related to NMR spectroscopy data for compound **1-SB3** can be found online at http://www.sciencedirect.com/science/article/pii/, doi:10.1016/j.dyepig.2011.10.014.

References

[1] O'Regan B, Grätzel M. A low-cost, high-efficiency solar cell based on dye-sensitized colloidal TiO_2 films. Nature 1991;335:737–40.
[2] (a) Hagfeldt A, Grätzel M. Light-induced redox reactions in nanocrystalline systems. Chem Rev 1995;95:49–68;
(b) Hagfeldt A, Grätzel M. Molecular photovoltaics. Acc Chem Res 2000;33:269–77;
(c) Grätzel M. Photoelectrochemical cells. Nature 2001;414:338–44;
(d) Park N-G, Kim K. Transparent solar cells based on dye-sensitized nanocrystalline semiconductors. Phys Status Solidi A 2008;205:1895–904;
(e) Grätzel M. Recent advances in sensitized mesoscopic solar cells. Acc Chem Res 2009;42:1788–98;
(f) Ardo S, Meyer GJ. Photodriven heterogeneous charge transfer with transition-metal compounds anchored to TiO_2 semiconductor surfaces. Chem Soc Rev 2009;38:115–64;
(g) Hagfeldt A, Boschloo G, Sun L, Kloo L, Pettersson H. Dye-sensitized solar cells. Chem Rev 2010;110:6595–663;
(h) Park N-G. Dye-sensitized metal oxide nanostructures and their photoelectrochemical properties. Korean J Chem Eng 2010;27:10–8.
[3] Nazeeruddin MK, Kay A, Rodicio I, Humphyr-Baker R, Müller E, Liska P, et al. Conversion of light to electricity by *cis*-X_2Bis(2,2′-bipyridyl-4,4′-dicarboxylate)-ruthenium(II) charge-transfer sensitizers (X = Cl^-, Br^-, I^-, CN^-, and SCN^-) on nanocrystalline TiO_2 electrodes. J Am Chem Soc 1993;115:6382–90.
[4] (a) Nazeeruddin MK, Zakeeruddin SM, Humphry-Baker R, Jirousek M, Liska P, Vlachopoulos N, et al. Acid-base equilibria of (2,2′-bipyridyl-4,4′-dicarboxylic acid)-ruthenium(II) complexes and the effect of protonation on charge-transfer sensitization of nanocrystalline titania. Inorg Chem 1999;38:6298–305;
(b) Nazeeruddin MK, Angelis FD, Fantacci S, Selloni A, Viscardi G, Liska P, et al. Combined experimental and DFT-TDDFT computational study of photoelectrochemical cell ruthenium sensitizers. J Am Chem Soc 2005;127:16835–47.
[5] (a) Nazeeruddin MK, Péchy P, Grätzel M. Efficient panchromatic sensitization of nanocrystalline TiO_2 films by a black dye based on a trithiocyanato-ruthenium complex. Chem Commun; 1997:1705–6;
(b) Nazeeruddin MK, Péchy P, Renouard T, Zakeeruddin SM, Humphry-Baker R, Comte P, et al. Engineering of efficient panchromatic sensitizers for nanocrystalline TiO_2-based solar cells. J Am Chem Soc 2001;123:1613–24.
[6] (a) Nazerruddin MK, Zakeeruddin SM, Lagref J-J, Liska P, Comte P, Barolo C, et al. Stepwise assembly of amphiphilic ruthenium sensitizers and their applications in dye-sensitized solar cell. Coord Chem Rev 2004;248:1317–28;
(b) Kuang D, Klein C, Ito S, Moser J-E, Humphry-Baker R, Evans N, et al. High-efficiency and stable mesoscopic dye-sensitized solar cells based on a high molar extinction coefficient ruthenium sensitizer and nonvolatile electrolyte. Adv Mater 2007;19:1133–7.
[7] (a) Mishra A, Fischer MKR, Bäuerle P. Metal-free organic dyes for dye-sensitized solar cells: from structure:property relationships to design rules. Angew Chem Int Ed 2009;48:2474–99;
(b) Ooyama Y, Harima Y. Molecular designs and syntheses of organic dyes for dye-sensitized solar cells. Eur J Org Chem; 2009:2903–34;
(c) Ning Z, Fu Y, Tian H. Energy Environ Sci 2010;3:1170–81.
[8] (a) Hara K, Sayama K, Ohga Y, Shinpo A, Suga S, Arakawa H. A coumarin-derivative dye sensitized nanocrystalline TiO_2 solar cell having a high solar-energy conversion efficiency up to 5.6%. Chem Commun; 2001:569–70;
(b) Hara K, Kurashige M, Dan-oh Y, Kasada C, Shinpo A, Suga S, et al. Design of new coumarin dyes having thiophene moieties for highly efficient organic-dye-sensitized solar cells. New J Chem 2003;27:783–5;
(c) Wang ZS, Cui Y, Hara K, Dan-oh Y, Kasada C, Shinpo A. A high-light-

harvesting-efficiency coumarin dye for stable dye-sensitized solar cells. Adv Mater 2007;19:1138–41.

[9] (a) Horiuchi T, Miura H, Uchida S. Highly efficient metal-free organic dyes for dye-sensitized solar cells. J Photochem Photobiol A 2004;164:29–32;
(b) Ito S, Miura H, Uchida S, Takata M, Sumioka K, Liska P, et al. High-conversion-efficiency organic dye-sensitized solar cells with a novel indoline dye. Chem Commun; 2008:5194–6;
(c) Matsui M, Ito A, Kotani M, Kubota Y, Funabiki K, Jin J, et al. The use of indoline dyes in a zinc oxide dye-sensitized solar cell. Dyes and Pigment 2009; 80:233–8.

[10] (a) Burke A, Schmidt-Medne L, Ito S, Grätzel M. A novel blue dye for near-IR 'dye-sensitized' solar cell applications. Chem Commun; 2007:234;
(b) Yum JH, Walter P, Huber S, Rentsch D, Geiger T, Nüesch F, et al. Efficient far red sensitization of nanocrystalline TiO_2 films by an unsymmetrical squaraine dye. J Am Chem Soc 2007;129:10320–1.

[11] (a) Liang M, Xu W, Cai F, Chen P, Peng B, Chen J, et al. New triphenylamine-based organic dyes for efficient dye-sensitized solar cells. J Phys Chem C 2007;111:4465–72;
(b) Ning Z, Zhang Q, Wu W, Pei H, Liu B, Tian H. Starburst triarylamine based dyes for efficient dye-sensitized solar cells. J Org Chem 2008;73:3791–7.

[12] Chen YS, Li C, Zeng ZH, Wang WB, Wang XS, Zhang BW. Efficient electron injection due to a special adsorbing group's combination of carboxyl and hydroxyl: dye-sensitized solar cells based on new hemicyanine dyes. J Mater Chem 2005;15:1654–61.

[13] Tan S, Zhai J, Fang H, Jiu T, Ge J, Li Y, et al. Novel carboxylated oligothiophenes as sensitizers in photoelectric conversion systems. Chem – Eur J 2005;11: 6272–6.

[14] (a) Edvinsson T, Li C, Pschirer N, Schöneboom J, Eickmeyer F, Sens R, et al. Intramolecular charge-transfer tuning of perylenes: spectroscopic features and performance in dye-sensitized solar cells. J Phys Chem C 2007;111: 15137–40;
(b) Li C, Yum JH, Moon SJ, Herrmann A, Eickemeyer F, Pschirer NG, et al. An improved perylene sensitizer for solar cell applications. ChemSusChem 2008; 1:615–8.

[15] (a) Borgström M, Blart E, Boschloo G, Mukhtar E, Hagfeldt A, Hammarströmand L, et al. Sensitized hole injection of phosphorus porphyrin into NiO: toward new photovoltaic devices. J Phys Chem B 2005;109: 22928–34;
(b) Eu S, Hayashi S, Umeyama T, Matano Y, Araki Y, Imahori H. Quinoxaline-fused porphyrins for dye-sensitized solar cells. J Phys Chem C 2008;112: 4396–405;
(c) Lee C-W, Lu H-P, Reddy NM, Lee H-W, Diau EW-G, Yeh C-Y. Electronically coupled porphyrin-arene dyads for dye-sensitized solar cells. Dyes Pigm 2011;91:317–23.

[16] Tang J, Hua J, Wu W, Li J, Jin Z, Long Y, et al. Energy Environ Sci 2010;3: 1736–45.

[17] Zhu W, Wu Y, Wang S, Li W, Li X, Chen J, et al. Adv Funct Mater 2011;21: 756–63.

[18] Ning Z, Zhang Q, Pei H, Luan J, Lu C, Cui Y, et al. J Phys Chem C 2009;113: 10307–13.

[19] (a) Ito S, Zakeeruddin SM, Humphry-Baker R, Liska P, Charvet R, Comte P, et al. High-efficiency organic-dye-sensitized solar cells controlled by nanocrystalline-TiO_2 electrode thickness. Adv Mater 2006;18:1202–5;
(b) Zhang G, Bala H, Cheng Y, Shi D, Lv X, Yu Q, et al. High efficiency and stable dye-sensitized solar cells with an organic chromophore featuring a binary π-conjugated spacer. Chem Commun; 2009:2198–200.

[20] (a) Kitamura T, Ikeda M, Shigaki K, Inoue T, Anderson NA, Ai X, et al. Phenyl-conjugated oligoene sensitizers TiO_2 solar cells. Chem Mater 2004;16: 1806–12;
(b) Thomas KRJ, Lin JT, Hsu Y-C, Ho K-C. Organic dyes containing thienyl-fluorene conjugation for solar cells. Chem Commun; 2005:4098–100;
(c) Hagberg DP, Edvinsson T, Marinado T, Boschloo G, Hagfeldt A, Sun L. A novel organic chromophore for dye-sensitizd nanostructured solar cells. Chem Commun; 2006:2245–7;
(d) Kim S, Lee JK, Kang SO, Ko J, Yum JH, Fantacci S, et al. Molecular engineering of organic sensitizers for solar cell applications. J Am Chem Soc 2006; 128:16701–7;
(e) Kim S, Choi H, Baik C, Song K, Kang SO, Ko J. Synthesis of conjugated organic dyes containing alkyl substituted thiophene for solar cell. Tetrahedron 2007;63:11436–43;
(f) Choi H, Baik C, Kang SO, Ko J, Kang MS, Nazeeruddin MK, et al. Highly efficient and thermally stable organic sensitizers for solvent-free dye-sensitized solar cells. Angew Chem Int Ed 2008;47:327–30;
(g) Qin H, Wenger S, Xu M, Gao F, Jing X, Wang P, et al. An organic sensitizer with a fused dithienothiophene unit for efficient and stable dye-sensitized solar cells. J Am Chem Soc 2008;130:9202–3;
(h) Lin JT, Chen P-C, Yen Y-S, Hsu Y-C, Chou H-H, Yeh M-CP. Organic dyes containing furan moiety for high-performance dye-sensitized solar cells. Org Lett 2009;11:97–100;
(i) Zhang F, Luo Y-H, Song J-S, Cuo X-Z, Liu W-L, Ma C-P, et al. Triphenylamine-based dyes for dye-sensitized solar cells. Dyes Pigm 2009;81:224–30 (j).

[21] (a) Hagberg DP, Yum JH, Lee H, De Angelis F, Marinado T, Karlsson KM, et al. Molecular engineering of organic sensitizers for dye-sensitized solar cell applications. J Am Chem Soc 2008;130:6259–66;
(b) Xu M, Li R, Pootrakulchote N, Shi D, Guo J, Yi Z, et al. Energy-level and molecular engineering of organic D–π–A sensitizers in dye-sensitized solar cells. J Phys Chem C 2008;112:19770–6;
(c) Shi D, Cao YM, Pootrakulchote N, Yi ZH, Xu MF, Zakeeruddin SM, et al. New organic sensitizer for stable dye-sensitized solar cells with solvent-free ionic liquid electrolytes. J Phys Chem C 2008;112:17478–85;
(d) Yum JH, Hagberg DP, Moon SJ, Karlsson KM, Marinado T, Sun LC, et al. A light-resistant organic sensitizer for solar-cell applications. Angew Chem Int Ed 2009;48:1576–80;
(e) Xu MF, Wenger S, Bala H, Shi D, Li RZ, Zhou YZ, et al. Tunig the energy level of organic sensitizers for high-performance dye-sensitized solar cells. J Phys Chem C 2009;113:2966–73;
(f) Zhang G, Bai Y, Li R, Shi D, Wenger S, Zakeeruddin SM, et al. Employ a bisthienothiophene linker to construct an organic chromophore for efficient and stable dye-sensitized solar cells. Energy Environ Sci 2009;2:92–5;
(g) He JH, Wu W, Hua J, Jiang Y, Qu S, Li J, et al. Bithiazole-bridged dyes for dye-sensitized solar cells with high open circuit voltage performance. J Mater Chem 2011;21:6054–62.

[22] (a) Hwang S, Lee JH, Park C, Lee H, Kim C, Park C, et al. A highly efficient organic sensitizer for dye-sensitized solar cells. Chem Commun; 2007:4887–9;
(b) Im H, Kim S, Park C, Jang S-H, Kim C-J, Kim K, et al. High performance organic photosensitizers for dye-sensitized solar cells. Chem Commun 2010; 46:1335–7.

[23] Grell M, Bradley DDC. Polarized luminescence from oriented molecular materials. Adv Mater 1999;11:895–905.

[24] (a) van Hal PA, Wienk MM, Kroon JM, Janssen RAJ. TiO_2 sensitized with an oligo(*p*-phenylenevinylene) carboxylic acid: a new model compound for a hybrid solar cell. J Mater Chem 2003;13:1054–7;
(b) Wienk MM, Kroon JM, Verhees WJH, Knol J, Hummelen JC, van Hal PA, et al. Efficient methano[70]fullerene/MDMO-PPV bulk heterojunction photovoltaic cells. Angew Chem Int Ed 2003;42:3371–5;
(c) Jang S-R, Lee C, Choi H, Ko JJ, Lee J, Vittal R, et al. Oligophenylenevinylene-functionalized Ru(II)-bipyridine sensitizers for efficient dye-sensitized nanocrystalline TiO_2 solar cells. Chem Mater 2006;18:5604–8;
(d) Tian HN, Yang XC, Chen RK, Zhang R, Hagfeldt A, Sunt LC. Effect of different dye baths and dye-structures on the performance of dye-sensitized solar cells based on triphenylamine dyes. J Phys Chem C 2008;112:11023–33;
(e) Kim C, Choi H, Kim S, Baik C, Song K, Kang M-S, et al. Molecular engineering organic sensitizers containing *p*-phenylenevinylene unit for dye-sensitized solar cells. J Org Chem 2008;73:7072–9.

[25] (a) Hara K, Dan-oh Y, Kasada C, Ohga Y, Shinpo A, Suga S, et al. Effect of additives on the photovoltaic performance of coumarin-dye-sensitized nanocrystalline TiO_2 solar cells. Langmuir 2004;20:4205–10;
(b) Koumura N, Wang Z-S, Mori S, Miyashita M, Suzuki E, Hara K. Alkyl-functionalized organic dyes for efficient molecular photovoltaics. J Am Chem Soc 2006;128:14256–7.

[26] Connelly NG, Geiger WE. Chemical redox agents for organometallic chemistry. Chem Rev 1996;96:877–910.

[27] (a) Jian H, Tour JM. Preparative fluorous mixture synthesis of diazonium-functionalized oligo(phenylenevinylene)s. J Org Chem 2005;70:3396–424;
(b) Ramesh AR, Thomas KG. Directional hydrogen bonding controlled 2D self-organization of phenyleneethynylenes: from linear assembly to rectangular network. Chem Commun 2010;46:3457–9.

[28] (a) Ahn T, Jang MS, Shim H-K, Hwang D-H, Zyung T. Blue electroluminescent polymers: control of conjugation length by kink linkages and substituents in the poly(*p*-phenylenevinylene)-related copolymers. Macromolecules 1999; 32:3279–85;
(b) Peeters E, van Hal PA, Knol J, Brabec CJ, Sariciftci NS, Hummelen JC, et al. Synthesis, photophysical properties, and photovoltaic devices of oligo(*p*-phenylenevinylene)-fullerene dyads. J Phys Chem B 2000;104:10174–90.

[29] Yi C, Blum C, Lehmann M, Keller S, Liu S-X, Frei G, et al. Versatile strategy to access fully functionalized benzodifurans: redox-active chromophores for the construction of extended π-conjugated materials. J Org Chem 2010;75: 3350–7.

[30] Yoshida M, Doi T, Kang S, Watanabe J, Takahashi T. Solid-phase combinatorial synthesis of ester-type banana-shaped molecules by sequential palladium-catalyzed carbonylation. Chem Commun; 2009:2756–8.

[31] (a) Goodbrand Hb, Hu N-X. Ligand-accelerated catalysis of the Ullmann condensation: application to hole conducting triarylamines. J Org Chem 1999; 64:670–4;
(b) Li R, Liu J, Cai N, Zhang M, Wang P. Synchronously reduced surface states, charge recombination, and light absorption length for high-performance organic dye-sensitized solar cells. J Phys Chem B 2010;114:4461–4.

[32] Li K, Qu J, Xu B, Zhou Y, Liu L, Peng P, et al. Synthesis and photovoltaic properties of novel solution-processable triphenylamine-based dendrimers with sulfonyldibenzene cores. New J Chem 2009;33:2120–7.

[33] Zhang J, Cui Y, Wang M, Liu J. Synthesis of double-conjugated-segment molecules and their application as ultra-broad two-photon-absorption optical limiters. Chem Commun; 2002:2526–7.

[34] (a) Park N-G, Kang MG, Ryu KS, Kim KM, Chang SH. Photovoltaic characteristics of dye-sensitized surface-modified nanocrystalline SnO_2 solar cells. J Photochem Photobiol A 2004;161:105–10;
(b) Yamaguchi T, Miyabe T, Ono T, Arakawa H. Synthesis of novel β-diketonate bis(bipyridyl) Os(II) dye for utilization of infrared light in dye-sensitized solar cells. Chem Commun 2010;46:5802–4.

[35] Frisch MJ, Trucks GW, Schlegel HB, Scuseria GE, Robb MA, Cheeseman JR, et al. Gaussian 09, revision B.01. Wallingford, CT: Gaussian, Inc.; 2010.
[36] (a) Lee C, Yang W, Parr RG. Development of the colle-salvetti correlation-energy formula into a functional of the electron density. Phys Rev B 1988;37:785–9;
(b) Becke AD. Density-functional thermochemistry. III. The role of exact exchange. J Chem Phys 1993;98:5648–52.
[37] Krishnan R, Binkley JS, Seeger R, Pople JA. Self-consistent molecular orbital methods. XX. A basis set for correlated wave functions. J Chem Phys 1980;72:650–4.
[38] (a) Lagemaat J, Park N-G, Frank AJ. Influence of electrical potential distribution, charge transport, and recombination on the photopotential and photocurrent conversion efficiency of dye-sensitized nanocrystalline TiO_2 solar cells: a study by electrical impedance and optical modulation techniques. J Phys Chem B 2000;104:2044–52;
(b) Kern R, Sastrawan R, Ferber J, Stangl R, Luther J. Modeling and interpretation of electrical impedance spectra of dye solar cells operated under open-circuit conditions. Electrochim Acta 2002;47:4213–25;
(c) Fabregat-Santiago F, Bisquert J, Garcia-Belmonte G, Boschloo G, Hagfeldt A. Influence of electrolyte in transport and recombination in dye-sensitized solar cells studied by impedance spectroscopy. Sol Energy Mater Sol Cells 2005;87:117–31;
(d) Wang Q, Moser J-E, Grätzel M. Electrochemical impedance spectroscopic analysis of dye-sensitized solar cells. J Phys Chem B 2005;109:14945–53;
(e) Lee K, Park SW, Ko MJ, Kim K, Park N-G. Selective positioning of organic dyes in a mesoporous inorganic oxide film. Nat Mater 2009;8:665–71.
[39] Hoshikawa T, Ikebe T, Kikuchi R, Eguchi K. Effects of electrolyte in dye-sensitized solar cells and evaluation by impedance spectroscopy. Electrochim Acta 2006;51:5286–94.
[40] Koo H-J, Park J, Yoo B, Yoo K, Kim K, Park N-G. Size-dependent scattering efficiency in dye-sensitized solar cell. Inorg Chim Acta 2008;361:677–83.
[41] Uam H-S, Jung Y-S, Jun Y, Kim K-J. Relation of Ru(II) dye desorption from TiO_2 film during illumination with photocurrent decrease of dye-sensitized solar cells. J Photochem Photobiol A Chem 2010;212:122–8.